Melting of Bimetallic Cu−Ni Nanoclusters

Shi-Ping Huang and Perla B. Balbuena*

Department of Chemical Engineering, University of South Carolina, Columbia, South Carolina 29208

Received: February 18, 2002; In Final Form: April 15, 2002

The thermal evolution of bimetallic Cu−Ni 343- and 1000-atom nanoclusters of compositions ($Cu_{0.25}Ni_{0.75}$) and ($Cu_{0.5}Ni_{0.5}$) is examined with molecular dynamics simulations using the Sutton-Chen many-body potential function. A heating curve is constructed starting from 0 K up to 1400 K, and the melting characteristics are determined on the basis of the variations of the potential energy and heat capacity with temperature. The shape evolution of the nanoclusters is analyzed in terms of deformation parameters. It is found that the bimetallic clusters melt in two stages. The first transition, corresponding to surface melting of the external Cu layers whereas the Ni core remains solid, is located at 400−500 K depending on the overall composition and cluster size. The second transition corresponds to homogeneous melting and takes place in the range of 700 to 900 K depending on the nanocluster size and composition. Thus, the melting temperature is much lower than those of bulk Cu and Ni, and the heat capacity shows a broader peak. At temperatures just before the melting transition, the heat capacity curves exhibit either a shoulder or an extra peak attached to the main melting transition peak; this is associated with isomerization structural transitions due to the diffusion of Cu atoms toward the cluster interior.

1. Introduction

Metal nanoparticles exhibit unusual chemical and physical properties different from those of the bulk metal, and have a number of fascinating potential applications in heterogeneous catalysts as well as microelectronic and optoelectronic devices.[1,2] Because of the large fraction of surface metal atoms present in nanoparticles ranging from 1 to 10 nm, their physical, chemical, and electronic properties are strongly dependent on their size, shape, and composition.[2] In particular, for supported or unsupported bimetallic nanoparticles widely used in the catalysis industry,[3,4] knowledge of their size and shape distribution, surface composition, and crystalline structure is essential for understanding their chemical and physical behavior, and may lead to improvements of their catalytic selectivity or activity.[2,3]

Research on the thermodynamic and kinetics of growth and stabilization of nanoparticles under thermal and stress effects is becoming of intense interest from the scientific and technological viewpoints.[2,5] In particular, the melting properties of nanoclusters and their effects on shape, composition, and sintering are needed in order to design efficient fabrication processes. Recent experiments[5−8] and molecular simulations[9−16] indicate that in nanoparticles within a certain range (from about 100 to 100 000 atoms, although the exact range depends on the metal), as the cluster size decreases the melting temperature and latent heat also decrease, and their values are much lower than the bulk values.[6,9,17,18] These phenomena can be understood considering that a large percentage of atoms residing on the surface of the cluster are weakly bound and less constrained in their thermal motion. A study of the melting, freezing, and coalescence of gold nanoclusters (135 to 3997 atoms) using molecular dynamics (MD) simulations indicated that there is a dynamical premelting of the outer layers which signals the proximity of the melting point, and pointed out that phenomenological sintering theories are unable to describe nanocluster aggregation.[12] The thermal evolution of structural and dynamics properties of gold nanocrystal clusters also analyzed with MD simulations[9] concluded that structural transformations (such as solid−solid transitions observed at low temperatures) are precursors to cluster melting. A dynamic solid−liquid coexistence was found in small Cu_n clusters ($n = 147$),[18] whereas bulk-type although broader transitions characterize slightly larger clusters ($n = 309$). The thermal behavior in small sodium clusters was analyzed with a combined density functional theory-MD approach; the calculated heat capacity curves indicated premelting (240 K) followed by homogeneous melting (270 K) in Na_{142} (an incomplete 3-shell icosahedron), whereas two well-separated transitions (130 K and 240 K) were observed for Na_{92}.[10,11] For Na_{55}, a complete 2-shell icosahedron, only one transition was found.[11] Recently, the potential energy distribution was used to investigate melting of transition-metal clusters.[19] It was shown that a surface-melted phase coexists with the solid core for clusters larger than 200 atoms, but no premelting peak was detected in heat capacity curves, thus the phase change was attributed to isomerization transitions, where the isomer energies are very similar.[19] On the other hand, very small clusters show a nonmonotonic variation of the melting temperature and latent heat with cluster size,[17,19] and complete-shell icosahedral clusters (such as 13, 55, 147 atoms) melt at higher temperatures than incomplete-shell sizes.[17] Also, recent experiments indicated that the melting temperature of tin cluster ions with 10−30 atoms lies above that of bulk metal, which is in line with the nonmonotonic behavior of the smallest clusters.[20]

Research focuses also on bimetallic nanoparticles using experimental techniques, such as electron microscopy and extended X-ray absorption fine structure[3,4] and theoretical methods.[4] The structural and thermal properties of $Cu_{n-x}Au_x$ ($n = 13, 14$) clusters were investigated using a constant-energy MD method, and it was suggested that the melting behavior of bimetallic clusters (Cu and Au) is strongly influenced by that of pure Cu clusters.[21] One interesting cluster melting process for a system containing a Pb core coated with Al was reported recently,[22] that suggested the existence of two melting mech-

* Corresponding author. E-mail: balbuena@engr.sc.edu.

10.1021/jp0204206 CCC: $22.00
Published on Web 06/29/2002

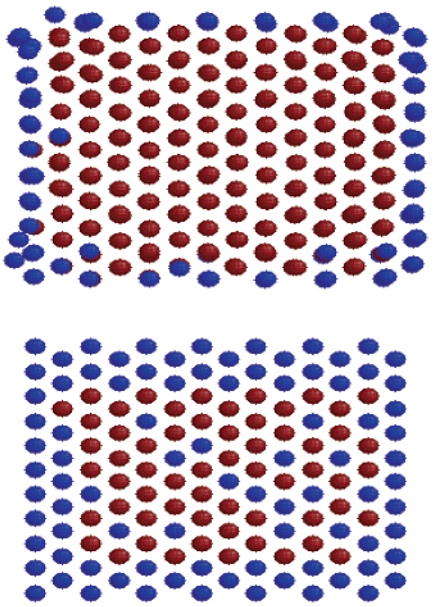

Figure 1. Nanoclusters initial structures at 0 K, where the blue atoms are Cu and the brown atoms are Ni. (a) $(Cu_{0.25}Ni_{0.75})_{343}$, (b) $(Cu_{0.5}Ni_{0.5})_{343}$.

anisms depending on the relative orientation of the core crystal structure with respect to that of the coating. In this paper we employ MD simulations using the Sutton-Chen many-body potential model to study the behavior of melting of Cu−Ni bimetallic clusters at two overall compositions and cluster sizes of 343 and 1000 atoms. The cluster sizes at 0 K (fcc crystals of approximately cubic shape) are 1.6 × 1.4 × 1.2 nm and 2.4 × 2.0 × 1.8 nm, respectively. We define deformation parameters to investigate the thermal behavior of the nanocluster, and discuss structural changes and atomic diffusion during the melting process.

2. Computational Details

2.1. Initial Configuration of the Clusters. The initial atomic distribution in all bimetallic nanoclusters in this study was obtained from Monte Carlo simulations based on the bond order simulation model,[23,24] where the site energy of any atom is assumed to be a function of the coordination and neighbor atomic type. Thus, the initial setting for our MD simulations consists of a cubic stack of layers with a face centered cubic (fcc) crystal structure, which expose fcc (111), (110), and (331) faces. In Cu/Ni systems, owing to the lower surface energy of Cu atoms, they tend to segregate to surface sites distributing first on low-coordination-number sites such as edge and corners.[25,26]

The MD simulations were performed at fixed mole fraction x and system size (n) of bimetallic nanoclusters $(Cu_xNi_{1-x})_n$. Figure 1a,b shows the nanocluster structure obtained from MC simulations[25,26] for $(Cu_{0.25}Ni_{0.75})_{343}$ and $(Cu_{0.5}Ni_{0.5})_{343}$, respectively. The nanocluster structure $(Cu_{0.25}Ni_{0.75})_{343}$ shown in Figure 1a contains 86 Cu and 257 Ni atoms. In its initial configuration, the surface is rich in Cu atoms since Cu has lower surface energy than Ni, whereas the Ni atoms form the nanocluster core. However, the number of Cu atoms is not enough to cover the nanocluster surface, which therefore contains also a few Ni atoms. MD simulations were also done on an equivalent overall composition system containing 250 Cu and 750 Ni atoms in order to study the size effect. A second nanostructure displayed in Figure 1b, $(Cu_{0.5}Ni_{0.5})_{343}$, includes 172 Cu and 173 Ni atoms, the Cu atomic fraction is approximately 0.5. In the initial configuration (Figure 1b) Cu atoms occupy all the surface sites, whereas the excess Cu along with most of the Ni atoms constitutes the nanocluster core.[25] The Cu surface segregation strongly depends on the crystallographic phase, for example for the case of Figure 1a, Cu atoms occupy totally the (110) phases, whereas on the (331) and (111) phases the Cu surface segregation is only partial. The choice of the cluster shape, sizes, and compositions in this study was based on the cases previously investigated, and their structures at 0 K do not necessarily correspond to global minima.

TABLE 1: Parameters of SC Potential

	a (Å)	ϵ (10^{-2} eV)	m	n	c
Cu−Cu	3.61	1.2386	6.0	9.0	39.755
Cu−Ni	3.56	1.3951	6.0	9.0	
Ni−Ni	3.52	1.5713	6.0	9.0	39.755

2.2. Molecular Dynamics Simulations. MD simulations are effective tools for understanding the melting process of finite systems at the atomistic level. In the simulation each particle is treated as a point mass governed by the classical equations of motion, and the thermodynamic and transport properties are obtained from time averages over the ensemble of particles. Many-body interatomic potentials, such as the embedded atom model[27,28] and the Sutton-Chen (SC) potential,[29] which include the effect of the local electronic density to account for many-body terms, are popular choices for fcc and other close-packed metal clusters. The SC potential has been used in Monte Carlo simulations to optimize transition-metal cluster structures and search for their global minimum.[30]

The general form of the SC potential can be expressed as

$$U_{\mathrm{tot}} = \epsilon\left[\frac{1}{2}\sum_{i\neq j}\sum\left(\frac{a}{r_{ij}}\right)^n - c\sum_i\sqrt{\rho_i}\right] \qquad (1)$$

The first term in eq 1 is a pairwise repulsive potential, the second term represents the metallic bonding energy associated with the local electron density ρ_i , defined as

$$\rho_i = \sum_{j\neq i}\left(\frac{a}{r_{ij}}\right)^m \qquad (2)$$

Here r_{ij} is the distance between atoms i and j, c is a dimensionless parameter, ϵ is a parameter with the dimensions of energy, and a is the fcc lattice constant. The square-root term of SC potential incorporates an attractive many-body contribution that has the same derivation as in the Finnis-Sinclair potential.[29] This potential model has proven being able to describe static and dynamic properties of transition and noble metals, such as bulk moduli and elastic constants,[29] as well as surface energies, stress tensor components, and surface relaxation of fcc metals.[31] A similar potential function has been developed for binary fcc metallic alloys and it was applied for calculating the concentration dependencies of the lattice parameters, elastic constants, and enthalpy of mixing of fcc binary alloys.[32]

We use the SC potential for the description of the interaction between atoms in the bimetallic nanoclusters, where the unlike parameters are obtained from the parameters for pure Cu and Ni.[32] The geometric mean was used to obtain the energy parameter ϵ^{CuNi} and the arithmetic mean for the length parameter a^{CuNi}. All parameters used in the MD simulations for calculating Cu−Ni bimetallic nanoclusters are listed in Table 1.

The MD simulations were carried out in a canonical ensemble at constant temperature T using the Berendsen thermostat,[33] with a temperature relaxation time of 0.4 ps, constant particle number

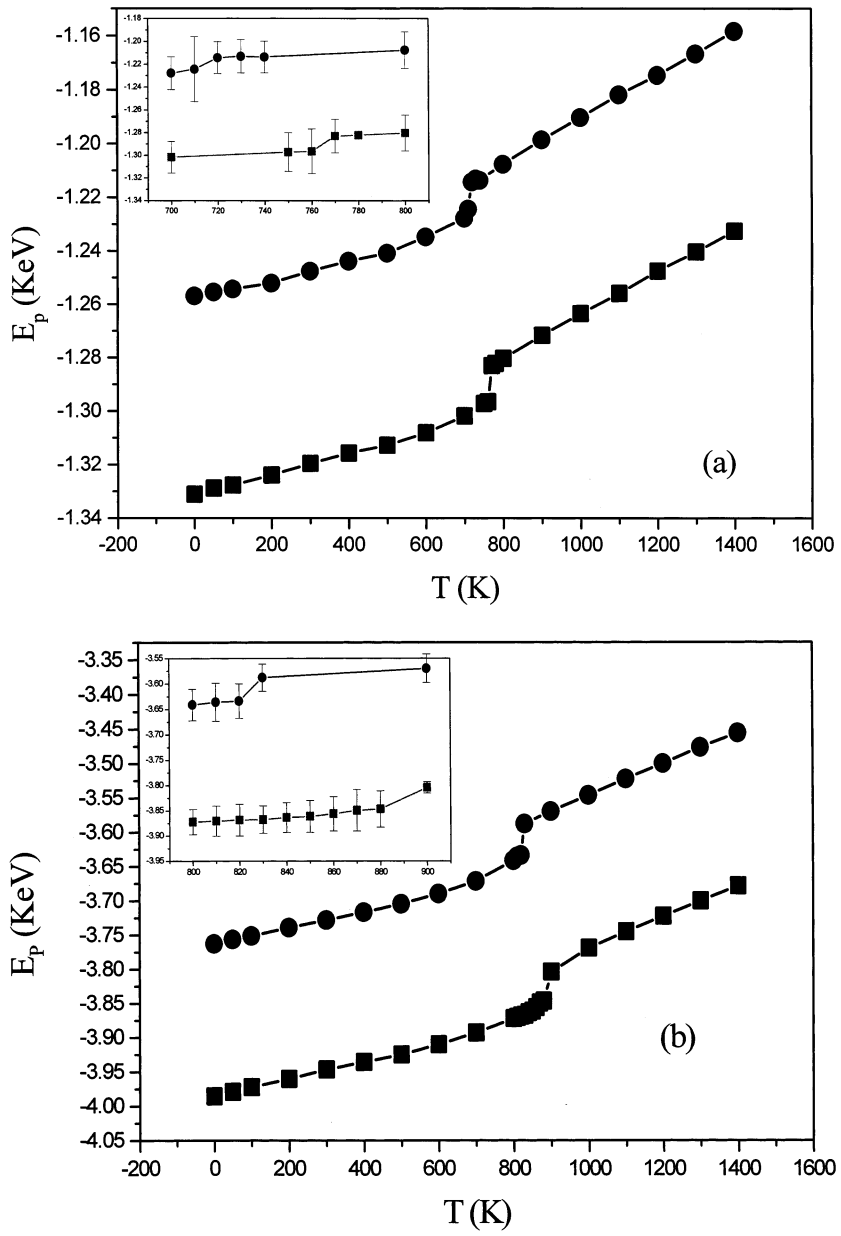

Figure 2. Calculated potential energy E_p (in keV) as a function of temperature. (a) Squares for $(Cu_{0.25}Ni_{0.75})_{343}$, circles for $(Cu_{0.5}Ni_{0.5})_{343}$; (b) squares for $(Cu_{0.25}Ni_{0.75})_{1000}$, circles for $(Cu_{0.5}Ni_{0.5})_{1000}$. Insets show error bars near the melting transitions.

N, and constant volume *V*, without periodic boundary conditions. The volume of the cubic simulation box is $(7L_x)^3$, where L_x = 17.5 Å is the side of the metallic cluster. The temperatures were varied in the range of 0 K to 1400 K, with temperature increments of 100 K, but approaching the melting point the increments were reduced to 10 K. We found temperature fluctuations of the order of 5 K at 50 K, increasing to 15 K at 100 K, and reaching the order of 75 K at temperatures near the melting transition. The equations of motion were integrated using the Verlet leapfrog method[33] with a time step of 0.001 ps. At each temperature, a total of 400 ps were run for equilibration and a production time of 200 ps was used for obtaining the average structural and dynamical properties. The calculations at each temperature were determined from the last configuration corresponding to the previous temperature. All calculations were performed using the program DL_POLY.[34]

The nanocluster structural features can be expressed through the atomic number distribution $N(z)$ along one of the coordinates axis. The atomic number distribution for each element is defined as

$$N_{Cu}(z) = \langle \sum_{i=1}^{n_{Cu}} \delta(z_i - z) \rangle \tag{3}$$

where n_{Cu} is the total number of Cu atoms in the cluster and the brackets represent the time average. To determine the melting temperature, the residual heat capacity C_v in the weak coupling (Berendsen thermostat method) ensemble[35] can be written as a function of the fluctuations in the potential energy $\langle(\delta E_p)^2\rangle$:

$$C_v = \frac{k_B\langle(\delta E_p)^2\rangle}{(k_B T)^2 - 2\alpha\langle(\delta E_p)^2\rangle/3N} \tag{4}$$

where α is the ratio of the standard deviations of the kinetic (*K*) and potential (E_p) energies,[35]

$$\alpha = \sqrt{\langle(\delta K)^2\rangle/\langle(\delta E_p)^2\rangle} \tag{5}$$

Using a value of 0.4 ps for the Berendsen coupling parameter

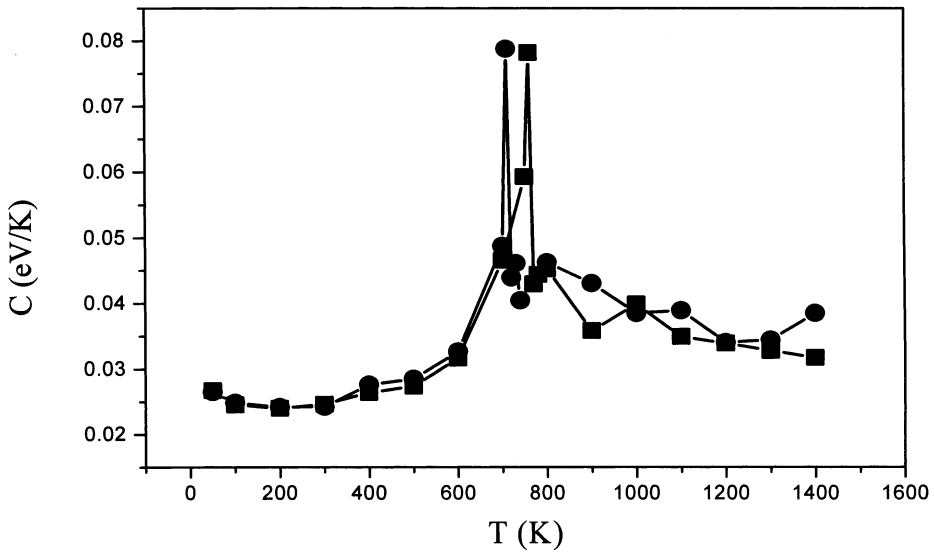

Figure 3. Specific heat at constant volume, eq 4, in eV/K, as a function of temperature. Squares: $(Cu_{0.25}Ni_{0.75})_{343}$; circles: $(Cu_{0.5}Ni_{0.5})_{343}$.

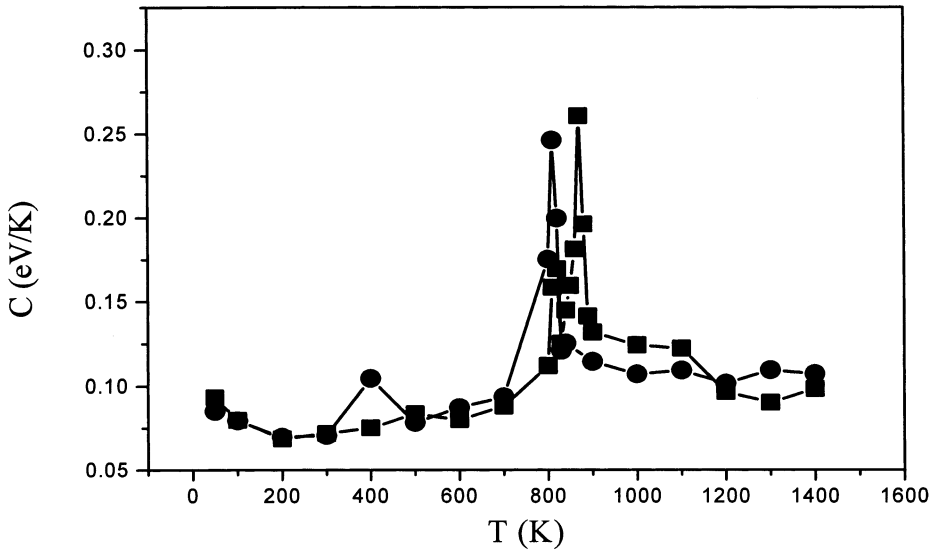

Figure 4. Specific heat at constant volume, eq 4, in eV/K, as a function of temperature. Squares: $(Cu_{0.25}Ni_{0.75})_{1000}$; circles: $(Cu_{0.5}Ni_{0.5})_{1000}$.

that determines the strength of the coupling to a heat bath,[35,36] we found that α is in all cases of the order of 10^{-4}, which determines that the specific heat calculated according to eq 4 is practically identical to that calculated in the canonical ensemble. In fact, as discussed extensively by Morishita,[35] the weak coupling ensemble approaches the canonical ensemble in the limit of $\alpha = 0$ (very short relaxation times) and the microcanonical ensemble in the limit of $\alpha = 1$ (long relaxation times).

The self-diffusion coefficient D is obtained from the mean square displacement:

$$D = \frac{1}{6\Delta t}\langle|(r_i(t+s) - r_i(s)|^2\rangle \qquad (6)$$

where $r_i(t + s)$ is the vector position of the ith atom, the average is over atoms of type i and over choices of the time origin s.

3. Results and Discussion

3.1. Thermodynamic Properties. Figure 2a shows the temperature dependence of the total potential energy for $(Cu_{0.25}Ni_{0.75})_{343}$ and $(Cu_{0.5}Ni_{0.5})_{343}$. It should be pointed out that when the heating and cooling curves are calculated or measured experimentally in finite systems, a hysteresis loop is found which is bounded by the freezing and melting temperatures.[13,16] Since we have not calculated the cooling curve, we observe that the total potential energy shows a simple jump as a function of temperature at the melting transition from the solid to the liquid state. To identify the melting temperature, the heat capacity at constant volume (eq 4) is shown in Figure 3. For $(Cu_{0.25}Ni_{0.75})_{343}$, the temperature interval where a jump in potential energy is observed (Figure 2a) is from 760 to 770 K, also corresponding to the maximum in the heat capacity curve (Figure 3, squares). Therefore, we estimate the melting temperature $T_{melt} = 760 \pm 10$ K. Similarly, the melting temperature of the nanocluster $(Cu_{0.5}Ni_{0.5})_{343}$ is 710 ± 10 K (Figure 3, circles). Owing to the higher Cu atomic fraction of $(Cu_{0.5}Ni_{0.5})_{343}$, its melting point is lower than that of $(Cu_{0.25}Ni_{0.75})_{343}$. At temperatures below the melting point, the behavior of the potential energy vs temperature is not totally smooth; there are changes in slope that are also reflected on the small peaks at 400 K in the heat capacity curves (Figure 3) which are indicators of Cu surface melting, as discussed below.

For larger nanoclusters, $(Cu_{0.25}Ni_{0.75})_{1000}$ and $(Cu_{0.5}Ni_{0.5})_{1000}$, their total potential energy curves are illustrated in Figure 2b, and their heat capacities in Figure 4. The melting temperatures

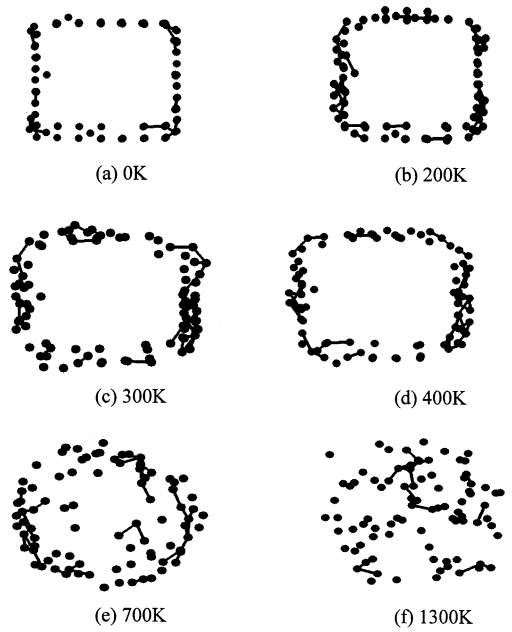

Figure 5. Cu atomic shells for $(Cu_{0.25}Ni_{0.75})_{343}$ at various temperatures during the heating process. (a) 0 K; (b) 200 K; (c) 300 K; (d) 400 K; (e) 700 K; (f) 1300 K.

T_{melt} estimated from Figure 4 are 870 ± 10 K and 810 ± 10 K for $(Cu_{0.25}Ni_{0.75})_{1000}$ and $(Cu_{0.5}Ni_{0.5})_{1000}$, respectively; they are 14% higher than those of the same composition 343-atom nanoclusters. In all cases, the nanocluster melting temperatures are much lower than those of experimental bulk Cu (T_{hm} = 1356.15 K)[37] and Ni (T_{hm} = 1726.15 K).[37] This is because in finite systems, due to the high ratio of surface to volume, the surface atoms have more freedom and experience weaker interactions compared with inside atoms, although, as described in the Introduction, nonmonotonic variations of the melting point with temperature are found in very small clusters of the order of tens of atoms.

Figures 3 and 4 depict small peaks in the heat capacity curve in the temperature range from 300 to 400 K, whereas a main peak is clearly displayed at a higher temperature (700 K − 900 K), this feature implies that the melting process takes place in two steps, surface melting and homogeneous melting, as it has been suggested.[9−11,14] Since the surface energy of Cu is lower than that of Ni, the majority of Cu atoms tend to enrich the surface,[25] however, in 343- and 1000-atom nanoclusters with an overall composition of 25% Cu, the number of Cu atoms is not enough to completely cover the whole surface for $(Cu_{0.25}Ni_{0.75})_{1000}$ nor for $(Cu_{0.25}Ni_{0.75})_{343}$. Therefore, the surfaces of these nanoclusters contain both Cu and Ni atoms, although most of the Ni atoms form the core. At higher overall compositions (such as the case of 50% Cu), Cu occupies the surface sites predominantly, and the core also contains some Cu atoms, although Ni mainly composes it.[26] Thus, in the solid phase, the nanocluster shape is cubic, and most of the Cu atoms occupy the surface. For $(Cu_{0.25}Ni_{0.75})_{343}$ and $(Cu_{0.50}Ni_{0.5})_{343}$, surface melting occurs at about T_{sm} = 400 K, whereas homogeneous melting is observed at T_{hm} = 760 K and T_{hm} = 710 K, respectively.

To understand the role of Cu atoms in these transitions, Figure 5 illustrates snapshots of the Cu atomic distribution in $(Cu_{0.25}Ni_{0.75})_{343}$ from 0 to 1300 K. At 300 and 400 K, it can be seen clearly that the Cu atoms are localized on the surface although a disordered pattern starts to appear. In the larger nanocluster (Figure 4) the surface melting takes place at different temperatures T_{sm} = 500 and 400 K. The higher surface melting temperature corresponds to the nanocluster with the lower percent of Cu atoms (Figure 4, squares), and for the same case there is a small peak right before the one corresponding to homogeneous melting. This feature was also reported based on MD and MC simulations of sodium clusters of sizes from 55 to 147 atoms, where it was related to isomerization transitions.[17] We did observe some changes in the density profiles and deformation parameters, discussed in a later section that can be associated with this phenomenon.

Figure 6 depicts the potential energy of $(Cu_{0.5}Ni_{0.5})_{343}$ as a function of the simulation time at temperatures near its melting point (T_{hm} = 710 ± 10 K). The fluctuations of the potential energy become stronger near the melting point (720 K). During the first 300 ps the potential energy is close to that in the solid phase (at 700 K), then it jumps to a higher energy corresponding to a value in the liquid-phase range (close to that at 800 K), and shows the first-order melting transition taking place.

3.2. Evolution of the Nanocluster Structure and Shape. Figure 7a,b shows the atomic number distribution function $N(x)$

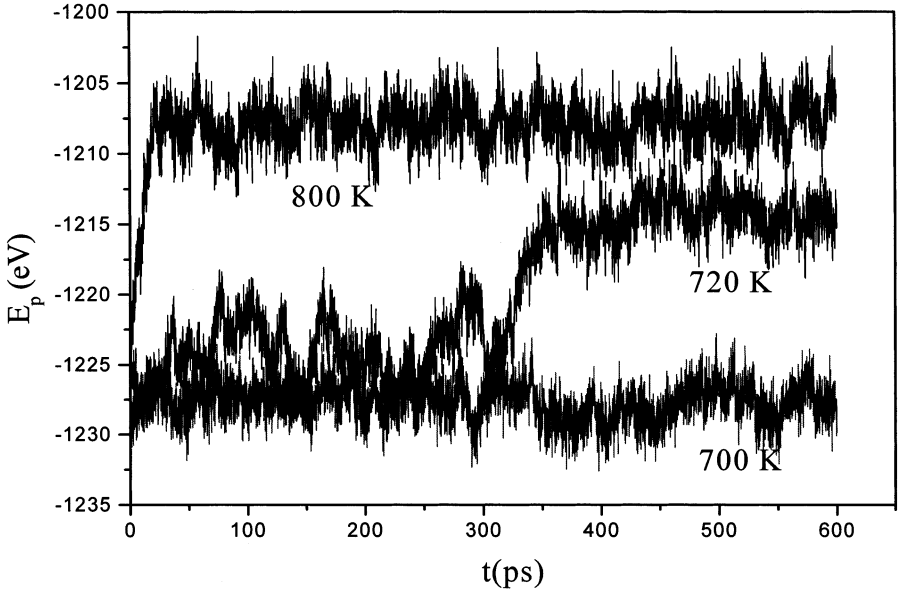

Figure 6. Time evolution of the potential energy near the melting point for $(Cu_{0.5}Ni_{0.5})_{343}$.

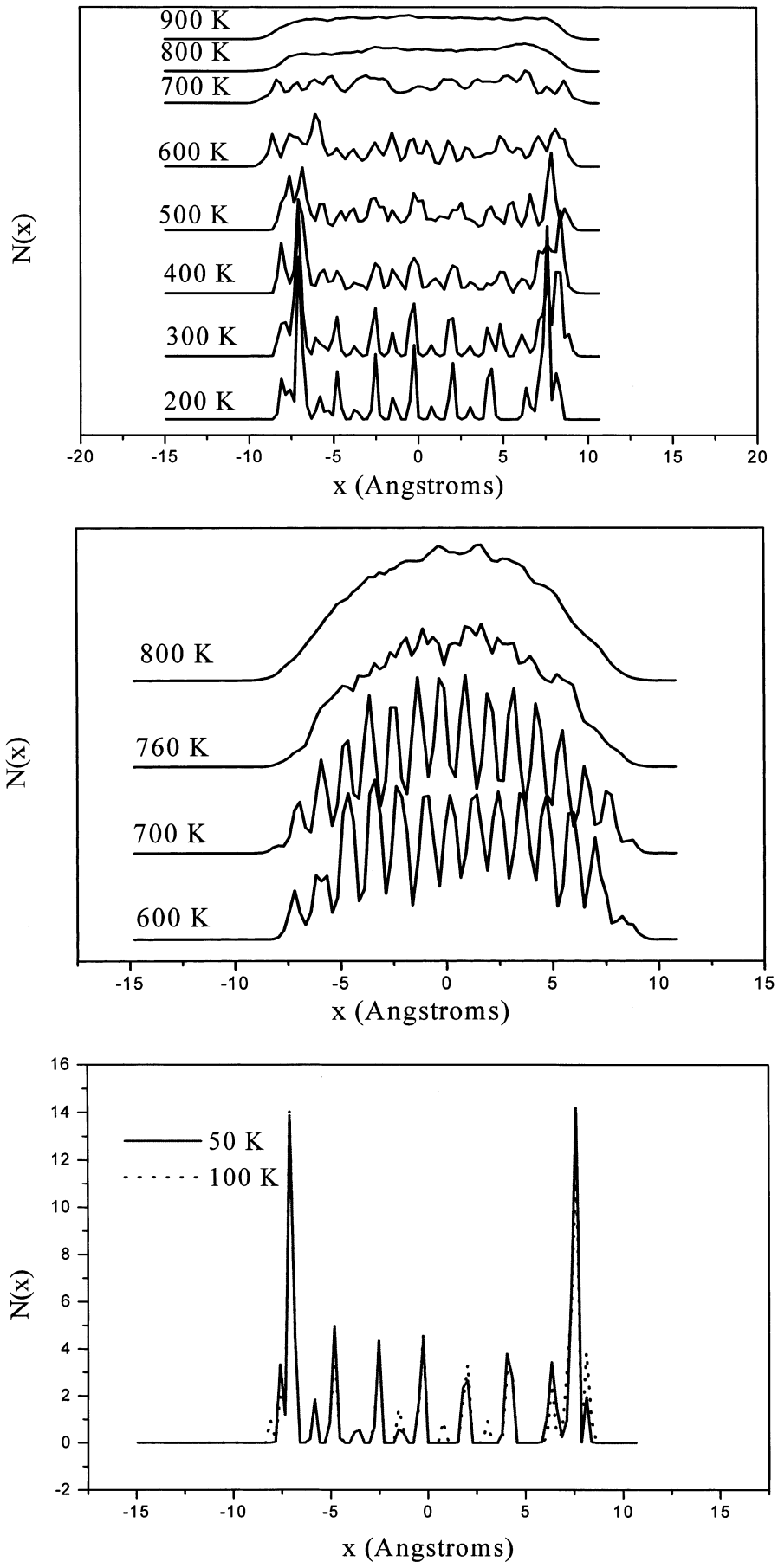

Figure 7. Number of atoms versus distance x (the cluster center of mass is located at $x = 0$), eq 3, for $(Cu_{0.25}Ni_{0.75})_{343}$. (a) Cu atomic distribution at various temperatures showing the melting transition; (b) Ni atomic distribution at temperatures below and above the melting transition; (c) Cu atomic distribution at 50 and 100 K.

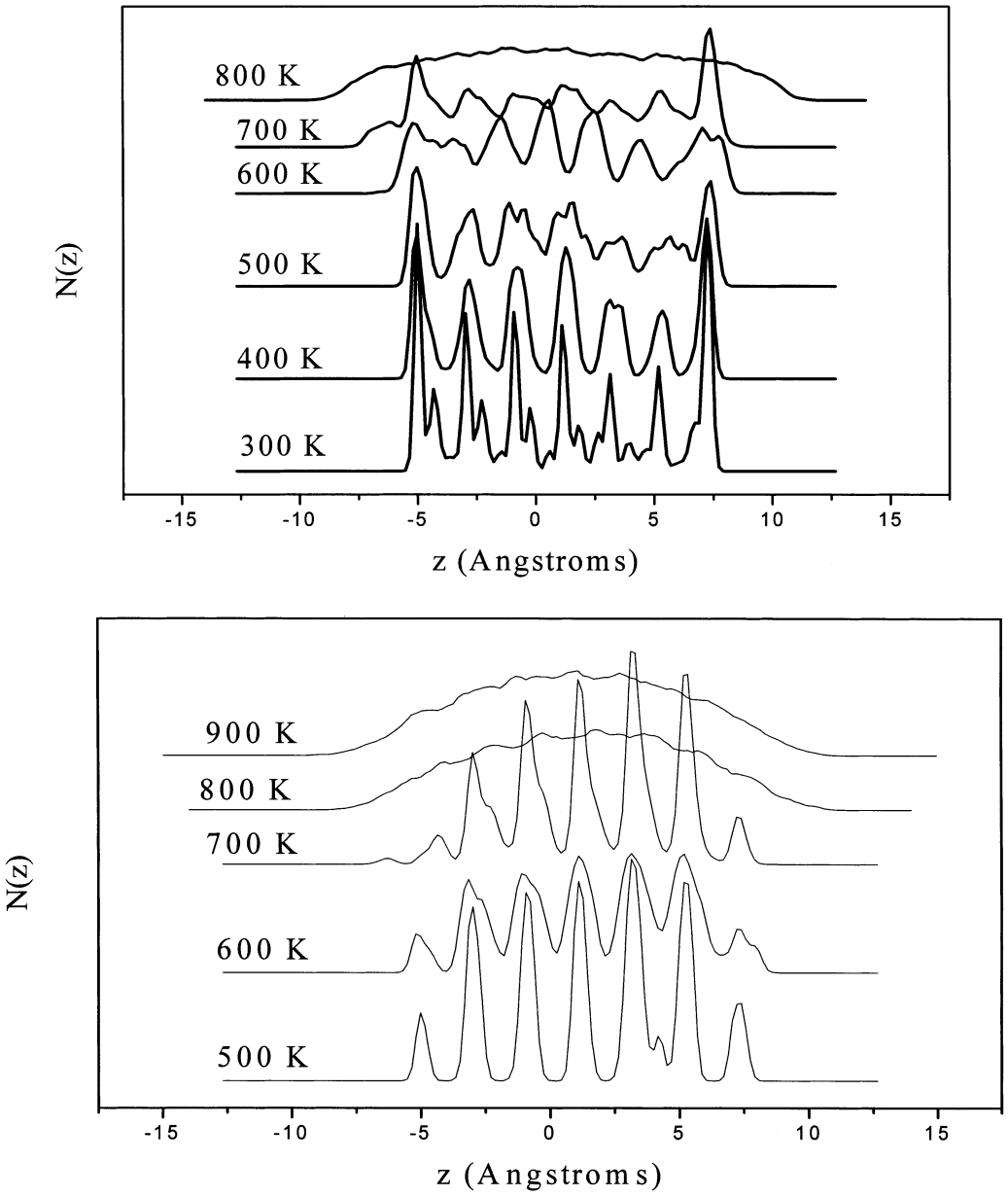

Figure 8. Number of atoms versus distance *z*, eq 3, for $(Cu_{0.5}\ Ni_{0.5})_{343}$. (a) Cu atomic distribution at various temperatures showing the melting transition; (b) Ni atomic distribution at temperatures below and above the melting transition.

for Cu and Ni, respectively, during the heating process for $(Cu_{0.25}Ni_{0.75})_{343}$, the *x* axis being the coordinate perpendicular to the (110) plane, where maximum Cu surface segregation is found. At very low temperatures this feature is clearly preserved as illustrated in Figure 7c. At temperatures below 400 K the Cu atomic shells still maintain a well-defined solidlike structure (Figure 5a−c). As temperature increases (Figure 7a), the surface melting process begins at about 400 K, evidenced by higher Cu atomic diffusion. Some small peaks merge and become broader, reflecting the initial surface melting process also indicated by the small jump detected in the heat capacity curve (Figure 3). The process develops further above 400 K, and is more clearly detected at 500 and 600 K, whereas at $T > 700$ K, the Cu profile shows liquid characteristics. In contrast, the atomic distribution for Ni is concentrated in the nanocluster core (Figure 7b), and retains its solid structure pattern until 700 K, but it becomes liquidlike for $T > 760$ K, which is our estimated homogeneous melting temperature for $(Cu_{0.25}Ni_{0.75})_{343}$. The Cu atomic diffusion toward the nanocluster core at temperatures approaching the melting point is visualized in Figure 5e,f.

Similar structural changes as a function of temperature are seen in Figure 8a,b for $(Cu_{0.5}Ni_{0.5})_{343}$. The surface melting of Cu atoms starts to be evident at $T > 300$ K (Figure 8a), by broadening of the peaks and by the diffusion of Cu atoms from the surface to the core which can be detected by the uniformity of the distribution. At 600 K both Cu and Ni profiles reflect structural changes (for example changes in the peak-to-peak distances) which may be due to an isomerization transition right before the melting transition. This isomerization is attributed to the substitution of Ni atoms in the core by Cu atoms that diffuse from the surface toward the cluster interior, as indicated by Figure 5c. On the other hand, most of the Ni atoms remain in their lattice positions corresponding to the solid structure at least until 700 K, as seen from Figure 8b, whereas at 800 K the Ni atomic distribution profile responds to a liquidlike system.

The nanocluster shape changes from cubic to spherical during the heating process. To explore the surface melting and nanocluster shape change, we define a deformation parameter[16] by

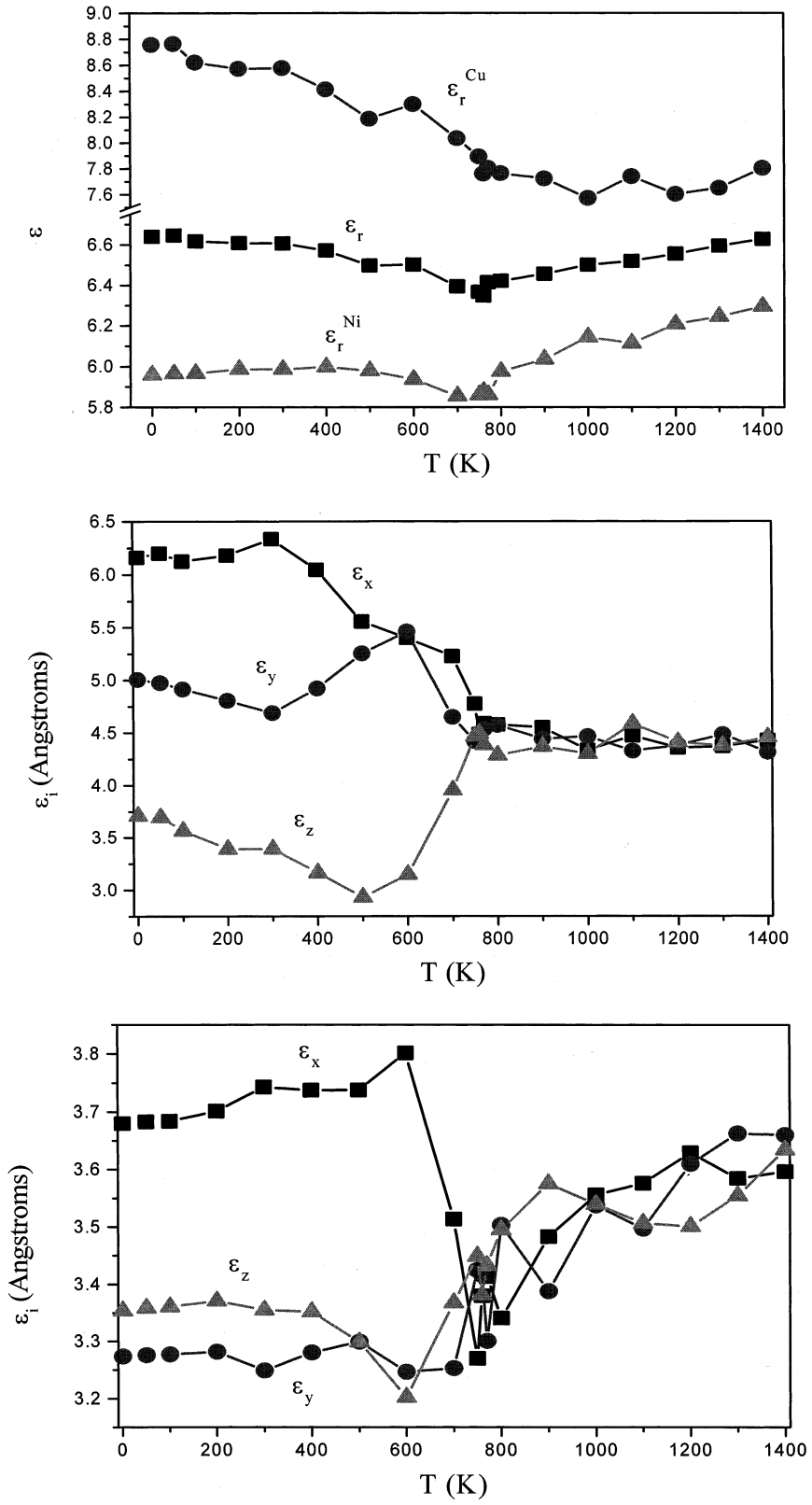

Figure 9. Deformation parameters, eqs 6 and 7, versus temperature for $(Cu_{0.25}Ni_{0.75})_{343}$. (a) Deformation parameters ϵ_r, ϵ_r^{Cu} and ϵ_r^{Ni}. (b) Cu atomic partial deformation parameter in *x*, *y*, and *z*. (c) Ni atomic partial deformation parameter in *x*, *y*, and *z*.

$$\epsilon_q = \frac{\sum_{i=1}^{N} |q_i - q_{cen}|}{N} \qquad (7)$$

where q_i stands for the coordinates of atom *i* either in the *x*, *y*, or *z* directions, or to the module of atom *i* position vector *r*(*x*, *y*, *z*), and q_{cen} is the cluster center of mass coordinate. The summation is over the *N* cluster atoms. The surface atoms behavior is very sensitive to changes of ϵ_q, whereas the interior atoms contribute much less. In this way we can establish a connection with the nanocluster shape when the melting process occurs. In a bimetallic nanocluster, the partial deformation parameter ϵ_q^X for each of the elements (X = Cu, Ni) can be

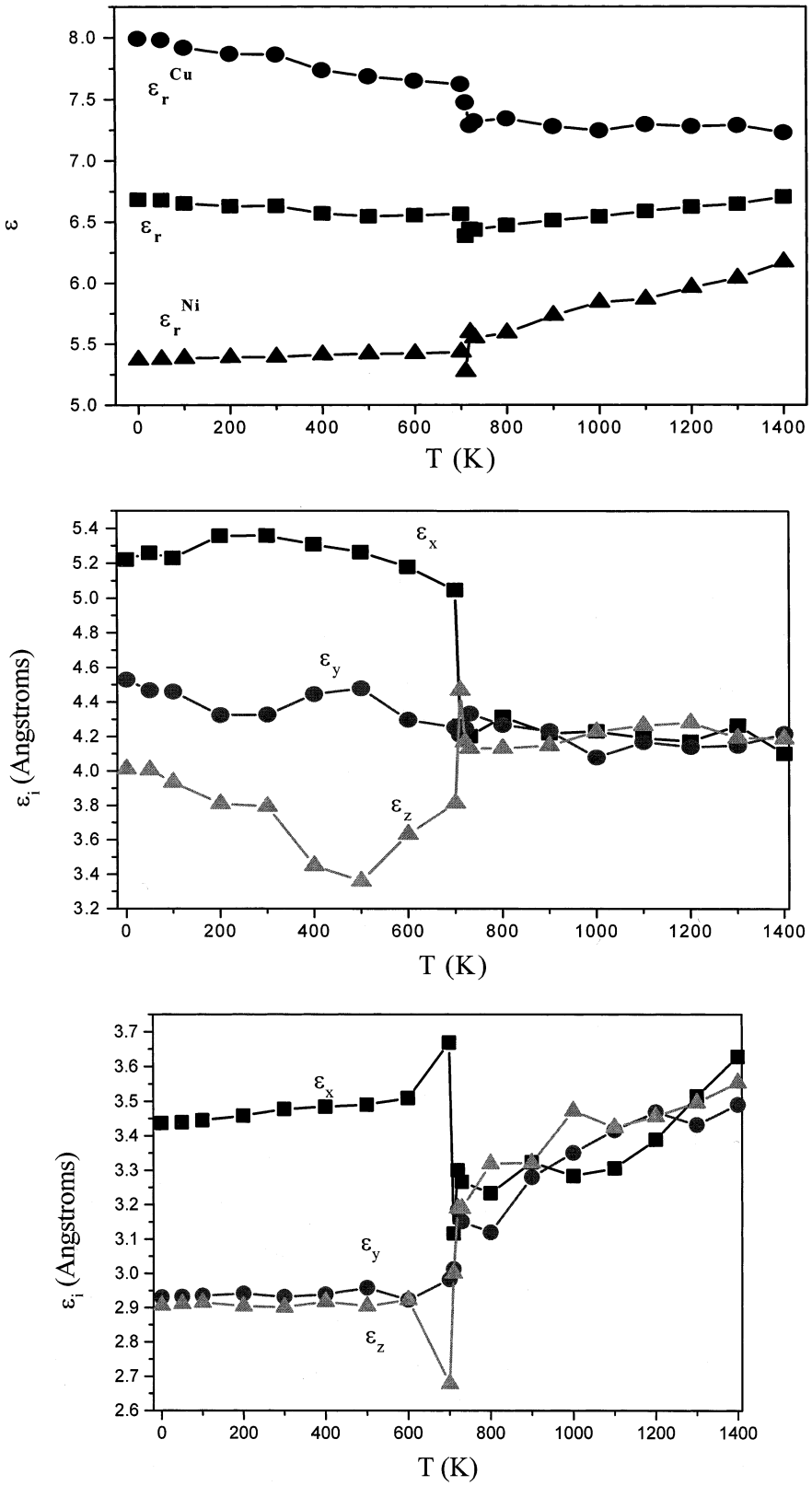

Figure 10. Deformation parameters, eqs 6 and 7, versus temperature for $(Cu_{0.5}Ni_{0.5})_{343}$. (a) Deformation parameters ϵ_r, ϵ_r^{Cu} and ϵ_r^{Ni}. (b) Cu atomic partial deformation parameter in *x*, *y*, and *z* directions. (c) Ni atomic partial deformation parameter in *x*, *y*, and *z* directions.

expressed as

$$\epsilon_q^X = \frac{\sum_{i=1}^{N_X} |q_i - q_{cen}|}{N_X} \qquad (8)$$

Figure 9a depicts the evolution of the deformation parameter ϵ_r in the radial direction with increasing temperature for $(Cu_{0.25}Ni_{0.75})_{343}$. ϵ_r decreases as *T* increases up to a temperature approaching the melting point 760 K. This is because of the diffusion of Cu atoms to the nanocluster core evidenced also by the sharp decrease in ϵ_r^{Cu} at temperatures below the melting

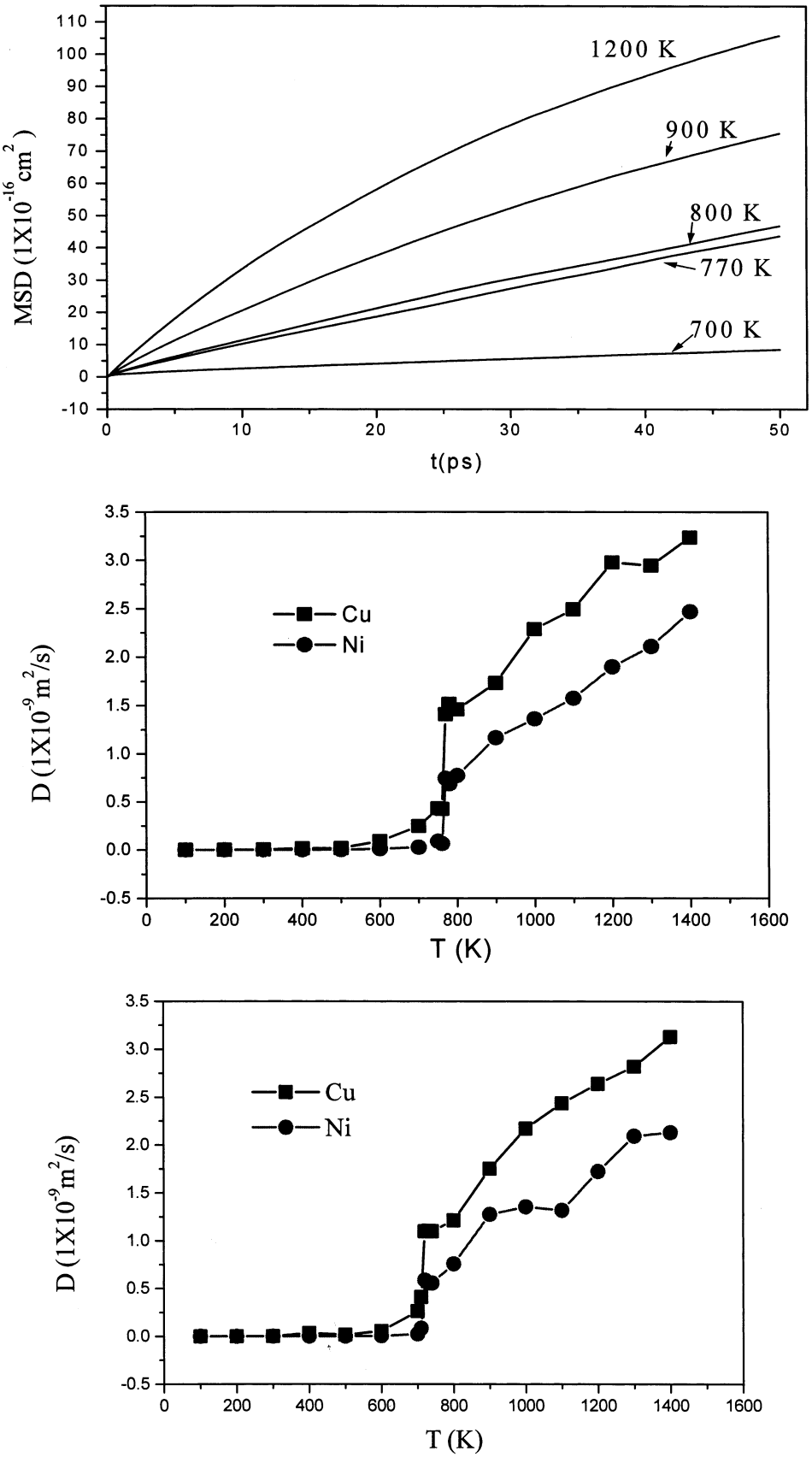

Figure 11. (a) Time dependence of the Cu mean square displacement (MSD) in $(Cu_{0.25}Ni_{0.75})_{343}$. (b) atomic self-diffusion coefficient for Cu and Ni in $(Cu_{0.25}Ni_{0.75})_{343}$; (c) atomic self-diffusion coefficient for Cu and Ni in $(Cu_{0.5}Ni_{0.5})_{343}$.

point. At higher temperatures ϵ_r shows a slight increase when *T* increases, indicating that the atoms tend to move away from the cluster center of mass as the structure becomes liquidlike. A similar behavior is observed for the Ni radial parameter (Figure 9a) at $T > 760$ K, whereas in the same range of temperatures the corresponding Cu parameter shows a decrease when *T* increases, because of the diffusion of Cu atoms toward the cluster center of mass.

The partial deformation parameters ϵ_q^{Cu} and ϵ_q^{Ni} are shown in Figure 9b,c for $q = x, y$, and z. The initial nanocluster shape (at low temperatures) is cubic with the side length (L) ordered according to $L_x > L_y > L_z$. Because of the atomic distribution in the bimetallic cluster, the Cu partial deformation parameters also show the same order $\epsilon_x^{Cu} > \epsilon_y^{Cu} > \epsilon_z^{Cu}$ (Figure 9b). During the initial heating process, at temperatures below 300 K (Figure 9b), the variation of the deformation parameters ϵ_q^{Cu} with temperature is small, a moderate decrease is observed in the y and z directions reflecting Cu atomic diffusion toward the center of mass. Above 300 K, and at temperatures increasing up to the melting point (760 K) a sharp decrease is observed in the deformation parameter in the x direction, also reflecting motion of Cu atoms toward the cluster interior. A similar behavior is found for Cu atomic displacements in the z direction, ϵ_z^{Cu} decreases steadily from 300 K up to 500 K, where there is a sharp increase in ϵ_z^{Cu} that coincides with a steady increase in the heat capacity curve in Figure 3a. This increase signals surface melting and is a precursor of a dramatic rise in the Cu atomic diffusion. The atomic motion may start first in the y direction where a sharp increase in ϵ_y^{Cu} is seen from 300 to 600 K. The motion in the Cu atomic shell is visualized in Figure 5c,d. Approaching the melting point, all partial deformation parameters become equal to each other, the thermal motion in the liquid phase causes them to fluctuate within a small range.

The corresponding activity in the Ni atomic motion as reflected by its partial deformation parameters is depicted in Figure 9c. There is a net correspondence between Figures 9b and 9c. Below 300 K, ϵ_q^{Ni} is practically constant in the three directions, the parameters are lower in magnitude than the Cu parameters since most of the Ni atoms are located in the nanocluster core, and the Ni atomic motion is small at low temperatures. Between 300 K and 600 K, slightly larger changes are detected, and these are possibly in response to the Cu atomic displacements. At 600 K, there is a sharp change in the Ni deformation parameters indicating higher Ni atomic motion, and above 760 K we observe a tendency of all parameters to become equal to a constant value, as found for ϵ_q^{Cu}.

Figure 10a−c shows the thermal behavior of the deformation parameters for $(Cu_{0.5}Ni_{0.5})_{343}$. The radial deformation parameters in Figure 10a are very stable at low temperatures, and well-defined changes are observed at temperatures close to the cluster melting point (710 K). The Cu partial deformation parameters (Figure 10b) indicate that surface melting starts at 300 K. In contrast, the Ni atomic deformation parameters in Figure 10c are practically constant below 600 K, where they experience large changes that reflect the beginning of the core melting process. In the liquid phase, the Cu atomic deformation parameters show small fluctuations around a fixed value, whereas the Ni parameters (Figure 10c), as observed from Figure 9c, evidence a clear liquidlike atomic motion driving the system away from the cluster center of mass.

3.3. Self-Diffusion Coefficient. The time evolution of the mean square displacement (MSD) for Cu atoms is illustrated in Figure 11a at several temperatures below and above the melting temperature, and the self-diffusion coefficient D calculated at each temperature from the slope of the MSD vs time (eq 6) is shown in Figure 11b,c for Cu and Ni atoms in $(Cu_{0.25}Ni_{0.75})_{343}$ and $(Cu_{0.5}Ni_{0.5})_{343}$, respectively. The self-diffusion coefficients in the solid phase ($T < 400$ K) are in the order of 10^{-16} to 10^{-13} m^2/s for Cu and 10^{-16} to 10^{-14} m^2/s for Ni. As T increases above 400 K, the Cu atomic diffusion coefficient gradually increases; however, until 700 K there is no clear signal indicating surface melting. A similar behavior is observed for the Ni atomic self-diffusion coefficient, although in contrast to Cu, the D_{Ni} values remain solidlike between 400 and 700 K. Close to the cluster melting point, both diffusion coefficients abruptly jump, reflecting the first-order melting transition. It is concluded that the average atomic diffusion coefficient is not as good an indicator of the premelting behavior as the specific heat or the deformation parameters; however, it shows very sharply the melting transition.

In the liquid-phase both diffusion coefficients fluctuate but tend to increase when temperature increases.

4. Conclusions

The melting behavior of bimetallic Ni−Cu nanoclusters of 343 and 1000 atoms is characterized by a premelting stage dominated by the diffusion of Cu atoms from the surface toward the center of the nanocluster, whereas the majority of the Ni atoms located in the cluster core retain their solid structure up to temperatures close to homogeneous melting. The melting transition in all nanoclusters in this study takes place at temperatures much lower than those corresponding to experimental bulk Cu and Ni crystals and its corresponding heat capacity peak is much broader than that found in bulk systems. A small peak in the heat capacity curves indicating surface melting occurs at temperatures below the melting transition, and at fixed overall composition, the surface melting temperatures are higher as the nanocluster size increases, because of the small proportion of Cu atoms residing in the surface as the cluster size increases. A small shoulder or a small additional peak is also found in the heat capacity curves at temperatures between those of surface and homogeneous melting, they are attributed to cluster isomerization transitions due to the diffusion of Cu atoms toward the nanocluster core and partial displacement of Ni atoms to periphery sites. Starting at 0 K, as the temperature increases the cluster initially contracts and tends to a spherical shape, whereas near the melting point, the mixing process of the bimetallic system dominates the nanocluster shape evolution.

The description of the melting transition from our simulations qualitatively agrees with previous simulated and real experiments (the most relevant to this work mentioned in the Introduction) and with purely theoretical discussions of phase transitions in small systems.[38,39] With the current and further expected advances on computational resources we are not that far from a full ab initio MD calculation[40] where the electronic effects are coupled to the nuclear motion and thus would provide a more complete picture of the phase transition.

Acknowledgment. This work is supported by the National Science Foundation Career Award Grant CTS-9876065, by the Army Research Office Grant No. DAAD19-00-1-0087, and by the Department of Energy/Basic Energy Sciences, Grant DE-FG02-1ER15249. The use of computational facilities at the National Energy Research Scientific Computing Center, NERSC, is gratefully acknowledged.

References and Notes

(1) Aiken, J. D., III; Finke, R. G. A review of modern transition-metal nanoclusters: their synthesis, characterization, and applications in catalysis. *J. Mol. Catal. A: Chem.* **1999**, *145*, 1.

(2) Bonnemann, H.; Richards, R. M. Nanoscopic metal particles—Synthetic methods and potential applications. *Eur. J. Inorg. Chem.* **2001**, 2455.

(3) Toshima, N.; Yonezawa, T. Bimetallic nanoparticles—novel materials for chemical and physical applications. *New J. Chem.* **1998**, 1179.

(4) Bromley, S. T.; Sankar, G.; Catlow, C. R. A.; Maschmeyer, T.; Johnson, B. F. G.; Thomas, J. M. New insights into the structure of supported bimetallic nanocluster catalysts prepared from carbonylated precursors: a

combined density functional theory and EXAFS study. *Chem. Phys. Lett.* **2001**, *340*, 524.

(5) Wang, Z. L.; Petroski, J. M.; Green, T. C.; El-Sayed, M. A. Shape transformation and surface melting of cubic and tetrahedral platinum nanocrystals. *J. Phys. Chem. B* **1998**, *102*, 6145.

(6) Kusche, R.; Hippler, T.; Schmidt, M.; Issendorff, B. V.; Haberland, H. Melting of free sodium clusters. *Eur. Phys. J. D* **1999**, *9*, 1.

(7) Schmidt, M.; Kusche, R.; Kronmuller, W.; Issendorff, B. V.; Haberland, H. Experimental determination of the melting point and heat capacity for a free cluster of 139 sodium atoms. *Phys. Rev. Lett.* **1997**, *99*, 99.

(8) Petroski, J. M.; Wang, Z. L.; Green, T. C.; El-Sayed, M. A. Kinetically controlled growth and shape formation mechanism of platinum nanoparticles. *J. Phys. Chem. B* **1998**, *102*, 3316.

(9) Cleveland, C. L.; Luedtke, W. D.; Landman, U. Melting of gold clusters: Icosahedral precursors. *Phys. Rev. Lett.* **1998**, *81*, 2036.

(10) Aguado, A.; Lopez, J. M.; Alonso, J. A. Melting in large sodium clusters: An orbital-free molecular dynamics study. *J. Phys. Chem. B* **2001**, *105*, 2386.

(11) Aguado, A.; Molina, L. M.; Lopez, J. M.; Alonso, J. A. Melting behavior of large disordered sodium clusters. *Eur. Phys. J. D* **2001**, *15*, 221.

(12) Lewis, L. J.; Jensen, P.; Barrat, J. L. Melting, freezing, and coalescence of gold nanoclusters. *Phys. Rev. B* **1997**, *56*, 2248.

(13) Qi, Y.; Cagin, T.; Johnson, W. L.; Goddard, W. A. Melting and crystallization in Ni nanoclusters: The mesoscale regime. *J. Chem. Phys.* **2001**, *115*, 385.

(14) Rodrigues, P. C. R.; Fernandes, F. M. S. Molecular dynamics of phase transitions in clusters of alkali halides. *Int. J. Quantum Chem.* **2001**, *84*, 169.

(15) Ercolesi, F.; Andreoni, W.; Tosatti, E. Melting of small gold particles: Mechanisms and size effects. *Phys. Rev. Lett.* **1991**, *66*, 911.

(16) Huang, S.-P.; Balbuena, P. B. Platinum Nanoclusters on Graphite Substrates: A Molecular Dynamics Study. *Mol. Phys.*, in press.

(17) Calvo, F.; Spiegelmann, F. Mechanisms of phase transitions in sodium clusters: From molecular to bulk behavior. *J. Chem. Phys.* **2000**, *112*, 2888.

(18) Lei, H. Melting of free copper clusters. *J. Phys: Condens. Matter* **2001**, *13*, 3023.

(19) Lee, Y. J.; Lee, E.-K.; Kim, S.; Nieminen, R. M. Effect of potential energy distribution on the melting of clusters. *Phys. Rev. Lett.* **2001**, *86*, 999.

(20) Shvartsburg, A. A.; Jarrold, M. F. Solid clusters above the bulk melting point. *Phys. Rev. Lett.* **2000**, *85*, 2530.

(21) Lopez, M. J.; Marcos, P. A.; Alonso, J. A. Structural and dynamical properties of Cu−Au bimetallic clusters. *J. Chem. Phys.* **1996**, *104*, 1056.

(22) Jin, Z. H.; Sheng, H. W.; Lu, K. Melting of Pb clusters without free surfaces. *Phys. Rev. B* **1999**, *60*, 141.

(23) Strohl, J. K.; King, T. S. A multicomponent, multilayer model of surface segregation in alloy catalysts. *J. Catal.* **1989**, *118*, 53.

(24) Zhu, L.; DePristo, A. E. Bond order simulation model: Coordination dependent bimetallic bonds. *J. Chem. Phys.* **1995**, *102*, 5342.

(25) Mainardi, D. S.; Balbuena, P. B. Monte Carlo Simulation Studies of Surface Segregation in Copper−Nickel Nanoclusters. *Langmuir* **2001**, *17*, 2047.

(26) Mainardi, D. S.; Balbuena, P. B. Surface Segregation in Bimetallic Nanoclusters: Geometric and Thermodynamic Effects. *Int. J. Quantum Chem.* **2001**, *85*, 580.

(27) Daw, M. S.; Baskes, M. I. Embedded-atom method: Derivation and application to impurities, surfaces, and other defects in metals. *Phys. Rev. B* **1984**, *29*, 6443.

(28) Foiles, S. M.; Baskes, M. I.; Daw, M. S. Embedded-atom-method functions for the fcc metals Cu, Ag, Au, Ni, Pd, Pt, and their alloys. *Phys. Rev. B* **1986**, *33*, 7983.

(29) Sutton, A. P.; Chen, J. Long-range Finnis-Sinclair potentials. *Philos. Mag. Lett.* **1990**, *61*, 139.

(30) Doye, J. P. K.; Wales, D. J. Global minima for transition-metal clusters described by Sutton-Chen potentials. *New J. Chem.* **1998**, 733.

(31) Todd, B. D.; Lynden-Bell, R. M. Surface and bulk properties of metals modeled with Sutton-Chen potentials. *Surf. Sci.* **1993**, *281*, 191.

(32) Rafii-Tabar, H.; Sutton, A. P. Long-range Finnis-Sinclair potentials for fcc metallic alloys. *Philos. Mag. Lett.* **1991**, *63*, 217.

(33) Allen, M. P.; Tildesley, D. J. *Computer Simulation of Liquids*; Oxford University Press: Oxford, 1990.

(34) Smith, W.; Forester, T. R. DL_POLY; Daresbury Laboratory: Daresbury, 1996.

(35) Morishita, T. Fluctuation formulas in molecular-dynamics simulations with the weak coupling bath. *J. Chem. Phys.* **2000**, *113*, 2976.

(36) Berendsen, H. J. C.; Postma, J. P. M.; Gunsteren, W. F. V.; Nola, A. D.; Haak, J. R. Molecular dynamics with coupling to an external bath. *J. Chem. Phys.* **1984**, *81*, 3684.

(37) *Handbook of Chemistry and Physics*, 77th ed.; Lide, D. R., Ed.; CRC Press: Boca Raton, FL, 1997.

(38) Cheng, H.-P.; Li, X.; Whetten, R. L.; Berry, R. S. Complete statistical thermodynamics of the cluster solid−liquid transition. *Phys. Rev. A* **1992**, *46*, 791.

(39) Hill, T. L. *Thermodynamics of small systems*; Dover: New York, 1994.

(40) Rytkonen, A.; Hakkinen, H.; Manninen, M. Melting and Octupole Deformation of Na_{40}. *Phys. Rev. Lett.* **1998**, *80*, 3940.